Journal of Fluid Science and Technology

Vol.3, No.8, 2008

# Mixing Enhancement and Interface Characteristics in a Small-Scale Channel*

Shuta NORO**, Kenji KOKUNAI**, Masaya SHIGETA***, Seiichiro IZAWA*** and Yu FUKUNISHI***

** Grad. School of Eng., Tohoku University
6-6-01 Aramaki-Aoba, Aoba-ku, Sendai 980-8579, Japan
E-mail: noro@fluid.mech.tohoku.ac.jp

*** Department of Mechanical Systems and Design, Tohoku University
6-6-01 Aramaki-Aoba, Aoba-ku, Sendai 980-8579, Japan

**Abstract**

The interface characteristics in a millimeter-scale channel are investigated in order to find a technique to speed up fluid mixing. The channel is fabricated on an acrylic-resin plate, where a cavity is attached in the downstream region of a T-shaped conduit. The mixing effect is evaluated using a blue dye and a colorless liquid, which are alternately injected into the channel by two syringe pumps. The important factors for highly efficient mixing under the combination of alternate inflow and cavity are investigated. Two-dimensional and three-dimensional numerical simulations are also performed, and the results are compared those of the experiment. It is confirmed that the fractal dimension and interface length inside a cavity can be used as indicators to predict the mixing level in the downstream region, although they are not perfect. The importance of focusing on both the stretching rate of the interface and the concentration gradient where the stretching of the interface occurs is presented.

*Key words* : Fluid Mixing, Millimeter-Scale Channel, Interface Length, Fractal Dimension, Concentration Gradient

## 1. Introduction

Thanks to the recent technological innovations of Micro-Electro-Mechanical-Systems (MEMS) and stereo-lithography, miniaturized systems highly integrated with micro-pumps, micro-sensors, and micro-actuators have been developed and widely applied in chemistry and biology fields[(1),(2)]. These systems, called Micro Total Analysis Systems ($\mu$-TAS) or Labs-on-a-Chip, have the benefit of reducing the amount of sample, expensive reagent, and waste production.

Generally, biochemical analyses require the complete mixing of two reactants before complex chemical syntheses can be carried out. Although the characteristic length associated with the micro devices decreases, some physical phenomena do not scale down linearly; mixing is a typical example. When the Reynolds number becomes extremely low, the diffusion due to turbulence ceases to exist and therefore cannot provide a means for sufficiently rapid mixing. For example, ink's coefficient of diffusion in water is on the order of $10^{-4}$ mm$^2$/s at room temperature, and the time constant for diffusion along a 1 mm length is $10^4$ s, which is quite large. The diffusion time increases even more when a certain protein exists in the solution as a reactant because the diffusion coefficient drastically decreases. Thus, the enhancement of mixing in such a small-scale environment is a key issue in the field of biochemical engineering.

A large number of micro mixers have been designed and investigated in the past. Ottino[(3)] provided an overview of mixing and chaotic advections. His research revealed three fundamental processes for mixing: (1) diffusion, (2) stretching and folding, and (3) adopting.

*Received 16 July, 2008 (No. 08-0480)
[DOI: 10.1299/jfst.3.1020]

Diffusion always takes place when a concentration gradient exists in a flow field. Mixing is also intimately related to stretching and folding, and adopting of material surfaces (or lines in two dimensions), which is generally caused by convection due to vortices. After a few repetitions of process (2) and (3), a finely striated structure appears and is prone to be rapidly smoothed out by molecular diffusion. These fluid motions provide a natural means of increasing the mixing efficiency in a turbulent flow. However, in a very small-scaled environment, the processes of stretching, folding, and adopting cannot generate turbulence. Therefore, most approaches to micro-mixers focus on increasing the interface between the fluids, in an effort to effectively increase molecular diffusion. Their strategies can be classified into two main categories, active and passive. Electromagnetic stirring[4], bubble-induced acoustic actuation[5], and ultrasonic effects[6] are examples of active mixing techniques, while lamination or rotation is used in passive mixers. Zigzag or twisted pipe[7]–[9] is an example. However, these devices often require the complicated control of external forces or a precise manufacturing of the flow channel. Mixing enhancements in channels with simple geometries have also been tested. Wong et al.[10] reported that a T-shaped (or Y-shaped) micro-mixer can shorten the mixing time within the range of milliseconds by increasing the Reynolds number to 400 ~ 500. In order to obtain the mean flow velocity of several meters, a very high pressure up to 6 bars was applied. Therefore, Wong et al. concluded that a large number of reactants and a high-pressure source are required for mixing.

This paper experimentally and numerically investigates the interface characteristics in a millimeter-scale channel are in order to obtain a principle guideline for micro-mixer design. The scale of our target flow field is up to sub-millimeters. Our previous studies have already revealed that mixing level can be improved when a cavity is attached to a normal T-shaped channel and a sinusoidal forcing is added to the inflows[11]–[13]. The mixing was evaluated using a blue dye and a colorless liquid, and the mixing level was judged based on the mixing variance coefficients along the streamwise and spanwise directions in the downstream region. This mixing enhancement was due to the lamination effect, in which the two liquids piled up on each other inside the cavity. However, the relation between the interface structure in the upstream region and the mixing level in the downstream region was not clear. Thus, the present study evaluates the quality of the interface structure inside a cavity using two indicators, a fractal dimension and an interface length. Also, this study searches for a factor that is essential for achieving highly efficient mixing.

## 2. Experiment and Numerical Approaches

### 2.1. Experiment Setup

The experiment apparatus is illustrated in Fig.1. Two syringe pumps are connected to the inlets of a mixing channel. One pump is filled with water colored with blue ink, and the other is filled with clear water. The motions of these pumps are controlled by a computer to adjust the flow rate and the timing. The channels are inscribed on the surface of an acrylic-resin plate by a milling machine. A silicon rubber sheet is placed between the acrylic-resin plates, one of which is inscribed to prevent the water from leaking.

As a preparatory experiment, a calibration is performed to determine the relationship between the brightness observed at each observational point and the mixing level. The mixing level is evaluated from the photographs of the flow, taken by a digital camera attached to a microscope at a location further downstream in the channel. Three LED lights are used for lighting. The shutter speed is fixed at 1/250 s; the aperture of the camera is fixed at $F = 5.6$; and the ISO is fixed at 80. The white balance is also fixed during the experiments.

### 2.2. Channel Geometry and Coordinate System

Figure 2 presents the channel geometries tested in the experiment. The straight part is 100 mm long, 1.0 mm wide and 0.4 mm deep. The origin of the coordinate system is set at the starting point of the mixing section, as indicated in Fig.1(a). The $x$ axis denotes the streamwise

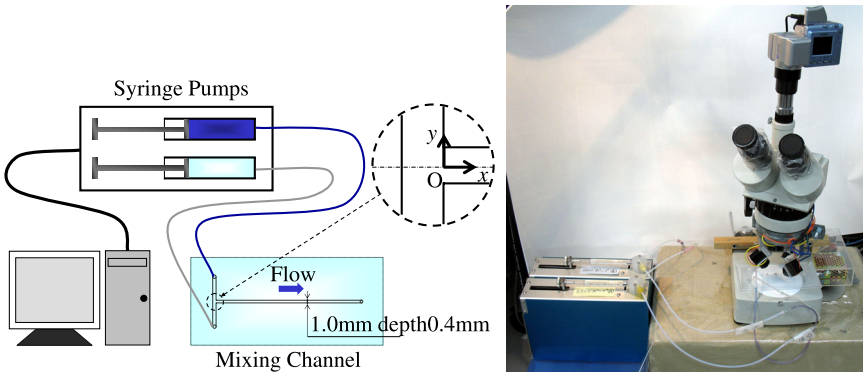


(a) Schematic view (b) Photograph

Fig. 1 Experiment apparatus.

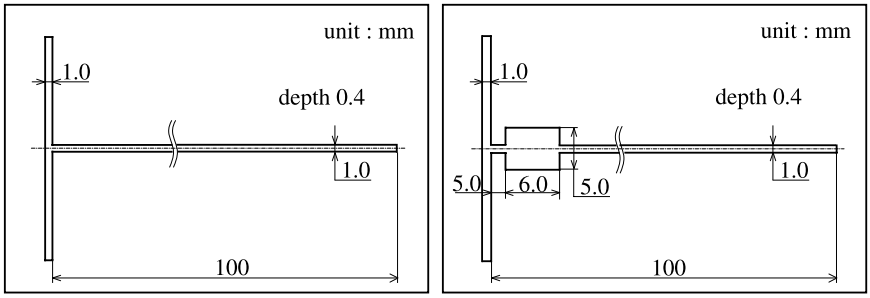


(a) Straight channel (Type T) (b) Channel with a cavity (Type C)

Fig. 2 Mixing channels.

direction, the $y$ axis denotes the spanwise direction, and the $z$ axis denotes the depth direction. Two types of channels are primarily tested: a simple straight channel (Fig.2 (a) Type T) and a channel with a cavity (Fig.2 (b) Type C). A square cavity (6.0 mm × 5.0 mm) is attached 5.0 mm downstream from the junction ($x$ = 0.0 mm). In addition, channels with several types of cavities are tested, as indicated in Fig.3: a symmetric cavity (Type SC), an asymmetric cavity (Type AC), a symmetric cavity with obstacles (Type SC-O), and an asymmetric cavity with obstacles (Type AC-O). Each cavity is located at $x$ = 5.0 mm. The size of the obstacle is 1.0 mm × 1.0 mm. The time period $T$ is set to 4.0 s, and the mean flow velocity $U$ is set to 5.0 mm/s.

### 2.3. Numerical Simulation

The velocity field and the concentration field are computed separately. First, the velocity field is computed by a finite-difference method. The governing equations are the incompressible Navier-Stokes equations and the continuity equation.

$$\left(\frac{\partial}{\partial t} + \boldsymbol{v}\cdot\nabla\right)\boldsymbol{v} = -\frac{1}{\rho}\nabla p + \nu\nabla^2\boldsymbol{v}, \tag{1}$$

$$\nabla\cdot\boldsymbol{v} = 0, \tag{2}$$

where $\boldsymbol{v}$ is the velocity vector, $\rho$ is the fluid density, $p$ is the fluid pressure, and $\nu$ is the kinematic viscosity. A second-order central-difference scheme is used for the spatial discretization of the pressure and the viscous terms. A third-order upwind scheme is applied to the convection term. Boundary conditions are shown in Tab.1, where the averaged velocity at the inlet is adjusted to represent the speeds of the syringe pumps. The fractional-step algorithm is adopted to couple the velocity and pressure fields. A staggered grid system is used. The time is advanced by the third-order Adams-Bashforth method.

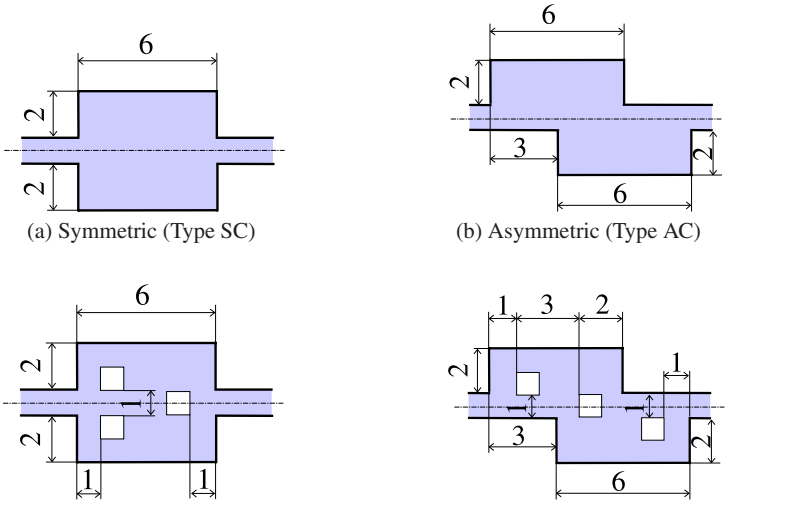


(a) Symmetric (Type SC) (b) Asymmetric (Type AC)

(c) Symmetric with obstacles (Type SC-O) (d) Asymmetric with obstacles (Type AC-O)

Fig. 3 Cavity geometries. (unit: mm)

Table 1 Boundary conditions.

| | Velocity field | Concentration field |
|---|---|---|
| Inflow | Dirichlet condition (given by the experiment results) | $\theta = 1$ for colored water, $\theta = 0$ for clear water |
| Outflow | First derivative is zero | Second derivative is zero |
| Wall | Non-slip | First derivative is zero |

Using previously obtained velocity data during one period of sinusoidal forcing the convection-diffusion equations

$$\left(\frac{\partial}{\partial t} + \boldsymbol{v}\cdot\nabla\right)\theta = D\nabla^2\theta, \tag{3}$$

are solved, where $\theta$ is the concentration and $D$ is the diffusion coefficient. The Cubic-Interpolated Pseudoparticle / Propagation (CIP)[14] method is applied to the convection term to accurately capture the interface between two liquids even when the concentration gradient is steep. The boundary conditions are shown in Tab.1.

Diffusion coefficient $D$ is chosen to agree with the experiment result, which is $D = 3.0 \times 10^{-4}$ mm$^2$/s. Two-dimensional and three-dimensional numerical simulations are conducted to investigate the behavior of the interface in detail.

There is a total of $766 \times 196$ (2D) and $307 \times 73 \times 9$ (3D) equi-spaced grid points. The kinematic viscosity $\nu$ given is that of a pure water, $1.0 \times 10^{-6}$ m$^2$/s.

### 2.4. Evaluation of Mixing Level

A modified Mixing Variance Coefficient method[11] is used to evaluate the mixing level of two liquids as follows,

$$\Phi_s = \frac{1}{N_t}\sum_{t=1}^{N_t}\Psi_s(\theta_{s,t}), \quad \Psi_s(\theta_{i,j}) = \frac{1}{N_s}\sum_{s=1}^{N_s}(\theta_{s,t} - \overline{\theta_s(t)})^2 \quad (0 \le \Phi_s \le 0.25) \tag{4}$$

$$\Phi_t = \frac{1}{N_s}\sum_{s=1}^{N_s}\Psi_t(\theta_{s,t}), \quad \Psi_t(\theta_{i,j}) = \frac{1}{N_t}\sum_{t=1}^{N_t}(\theta_{s,t} - \overline{\theta_t(s)})^2 \quad (0 \le \Phi_t \le 0.25) \tag{5}$$

$$\overline{\theta_s(t)} = \frac{1}{N_s}\sum_{s=1}^{N_s}\theta_{s,t}, \qquad \overline{\theta_t(s)} = \frac{1}{N_t}\sum_{t=1}^{N_t}\theta_{s,t}. \tag{6}$$

The spatial and temporal variances ($\Phi_s$, $\Phi_t$) are calculated to evaluate the streamwise and spanwise changes in the flow. Both indicators take values within $0 \le (\Phi_s, \Phi_t) \le 0.25$. Figure

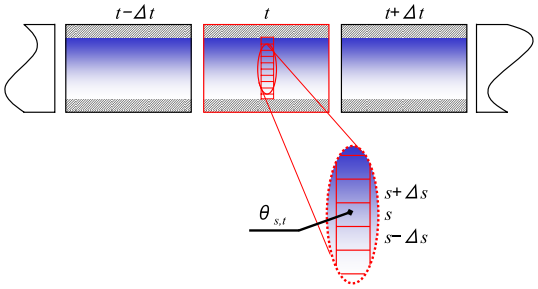


Fig. 4 Observation boxes.

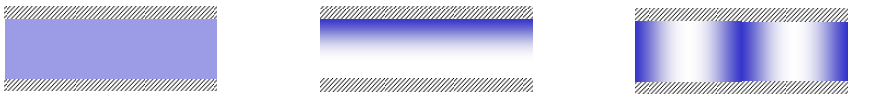

(a) $\Phi_s = \Phi_t \simeq 0$ (well mixed) (b) $\Phi_t \ll \Phi_s$ (parallel) (c) $\Phi_s \ll \Phi_t$ (vertical stripe)

Fig. 5 Relation between ($\Phi_s$, $\Phi_t$) and typical flow patterns.

4 shows the observation boxes. The images of the magnified observation area are captured at a frame rate of 30 fps. There are 20 boxes along the $y$ axis $N_s$. The number of samples for one period $N_t$ is 120, which is the product of $T = 4.0$ s and the frame rate. Figure 5 presents the relation between these two parameters and typical flow patterns, well-mixed, parallel, and alternating flows. When $\Phi_s$ is large, the contours representing the mixing levels become parallel to the sidewalls and similar to those without forcing. When $\Phi_t$ is large, a vertical stripe pattern appears. If a flow is well mixed and the concentration is uniform, both parameters approach zero. $\Phi_s$ and $\Phi_t$ are sensitive to the variance of concentration in the wall-normal and the streamwise directions.

The fractal dimension $Ds$ is given by

$$Ds = \lim_{h \to 0} \frac{\log(N(h))}{\log(1/h)} \tag{7}$$

where $N(h)$ is the number of objects of size $h$ needed to cover the original object. $Ds$ is a measure of the self-similarity of a figure. For example, when a line with a finite length is divided into two parts of the same length, $Ds = \log 2^n / \log 2^n = 1$. So the fractal dimension of the straight line is 1. In a similar way, $Ds = \log 4^n / \log 2^n = 2$ for a square, and $Ds = \log 8^n / \log 2^n = 3$ for a cube. $Ds$ is a generally $0 \leq Ds \leq 3$, where $Ds = 0$ is the dimension of a point. In this study, the fractal dimension is estimated by the box-counting method.

## 3. Results and Discussion

### 3.1. Comparison between Up-stream and Down-stream Regions

The flow patterns obtained by the experiment and the two-dimensional simulation are depicted in Fig.6. When the blue water and clear water alternately flow into the cavity, their speeds decrease as they spread in the spanwise direction (Type SC and AC). By piling up, they generate a striped pattern inside the cavity. As a result, compared with the normal straight channel, the interface between two liquids becomes longer and thinner inside the cavity, especially for Type SC-O and AC-O. Both experiment and numerical results reveal similar flow patterns, though the interfaces in the experiment are blurry. The blurred image of the interface in the experiment is due to the experiment setup. The captured images, taken from above by a digital camera connected to a microscope, include all information in the depth direction. The effect of the observation procedures on the concentration measurements is discussed later.

Figure 7 presents the fractal dimension $Ds$ and the interface length measured inside the cavity, where the interface length is obtained by the sum of lengths of the contour lines of selected mixing ratios (i.e. $\theta = 0.3$, 0.4, 0.5, and 0.6). Both values are averaged in time for one forcing period $T$. The experiment and numerical results indicate a similar tendency: the

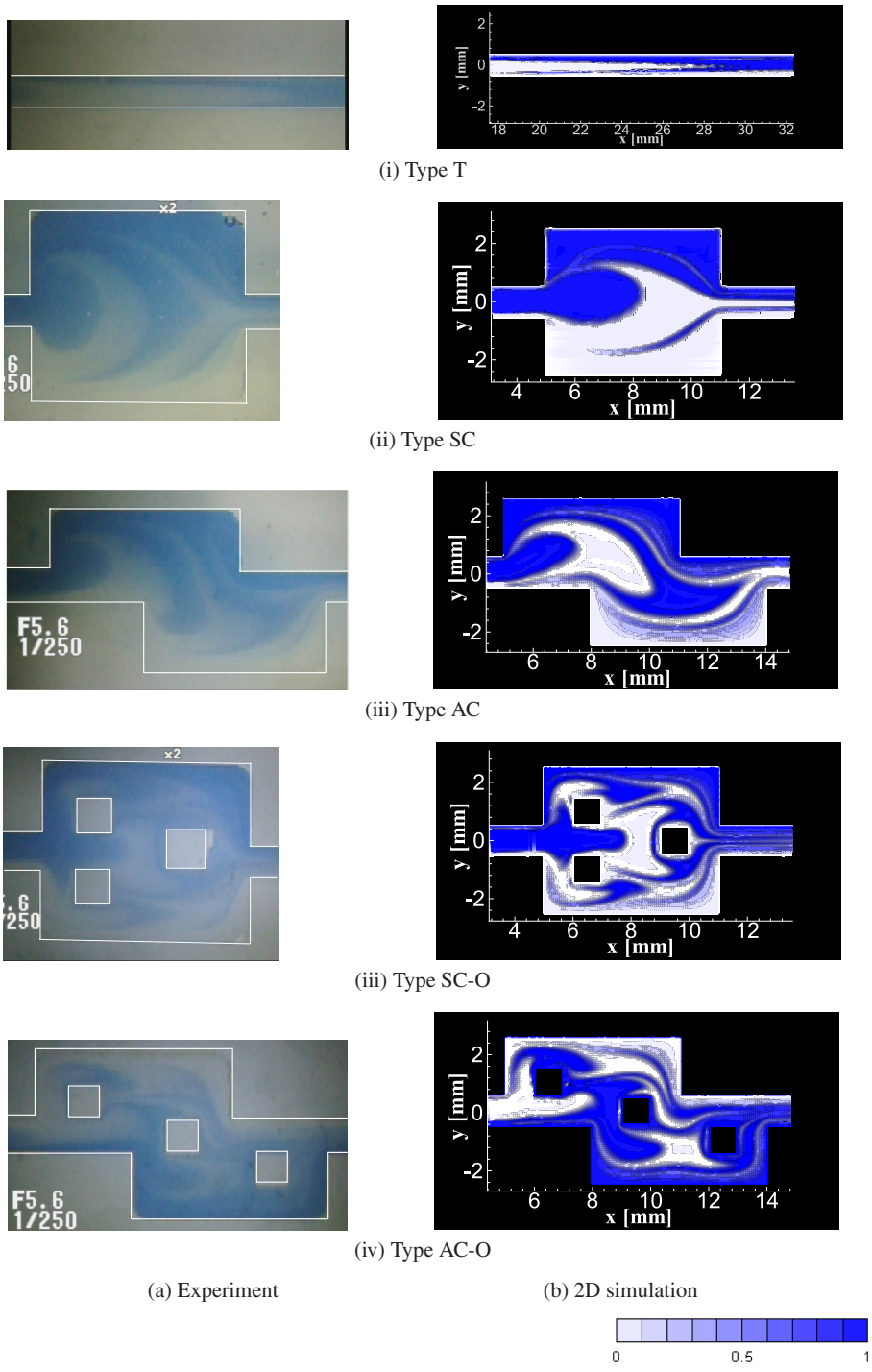


Fig. 6 Comparison of the flow patterns in various channels.

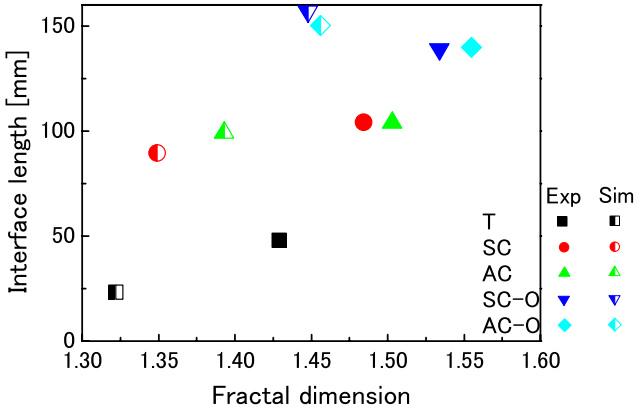


Fig. 7 Fractal dimension and interface length.

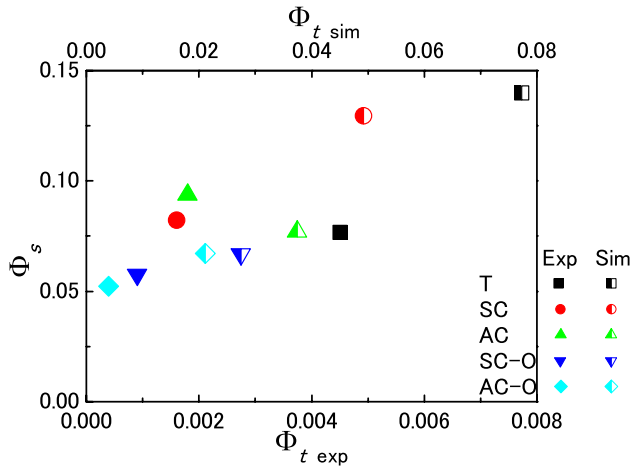


Fig. 8 Mixing variance at $x$ = 45 mm.

total length of the contour lines increases with the presence of the cavity, especially when the obstacles are inside the cavity, and the fractal dimensions are proportional to the interface lengths. Corresponding mixing levels in the downstream region at $x$ = 45 mm are indicated in Fig.8. Where the interface lengths are greater or the fractal dimensions are higher inside the cavity, the mixing in the downstream region is found to be better. It should be noted that the mixing level is remarkably improved by adding obstacles inside the cavity. The results reveal that the interface length and the fractal dimension in the upstream region can be useful indicators to predict the mixing level in the downstream region.

### 3.2. Comparison between Experiment and Simulation

Although qualitative agreement between the experimental results and the numerical results can be observed in Fig.8, the values of $\Phi_t$ in the simulation are ten times larger than those in the experiment. Because such a large discrepancy may occur in the three-dimensionality of the flow, a three-dimensional computation is carried out.

Figure 9 reveals the three-dimensional numerical simulation results, which are computed under the same conditions as the experiment results. Flow pattern (a) is obtained by averaging the concentration values in the depth direction, simulating the experiment, while pattern (b) represents the concentration profile in the $x$-$y$ section at the center of the channel, $z$ = 0 mm. Compared with the two-dimensional simulation (Fig.6 b-ii), the colored water entering the cavity spreads more in the spanwise direction, forming a mushroom-like shape. The interface

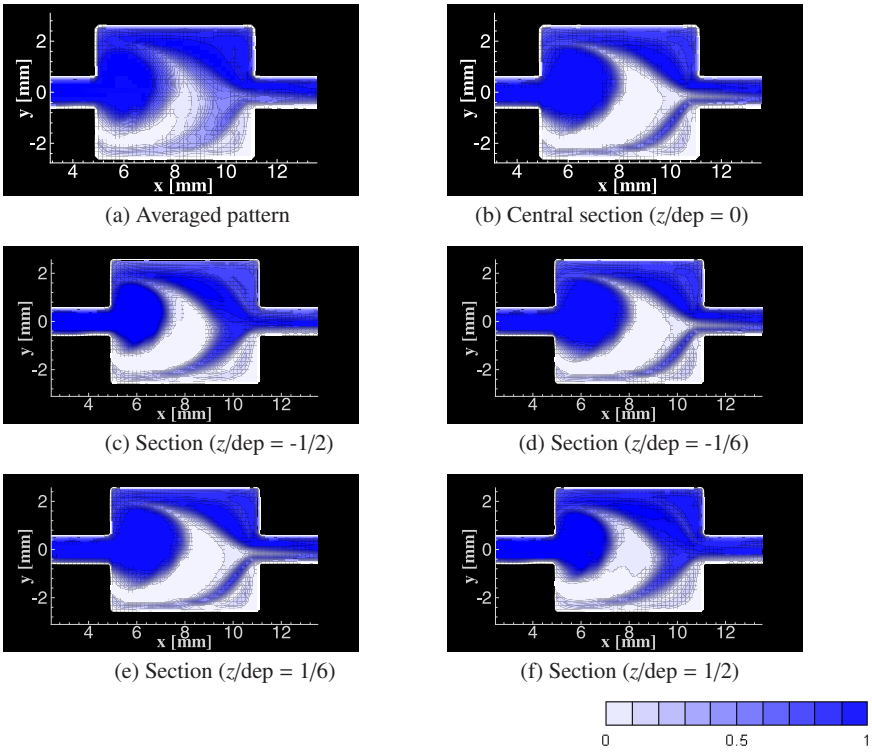


(a) Averaged pattern (b) Central section ($z$/dep = 0)

(c) Section ($z$/dep = -1/2) (d) Section ($z$/dep = -1/6)

(e) Section ($z$/dep = 1/6) (f) Section ($z$/dep = 1/2)

Fig. 9 Comparison of the flow patterns.

of (a) becomes as blurry as the experiment result in Fig.6 a-ii.

Figure 10 presents the mixing levels in the streamwise direction at $x$ = 20, 30 and 45 mm for each case. The mixing level of the averaged view of the three-dimensional simulation is very close to that indicated in the experiment results, Although the flow patterns obtained by the two-dimensional computations and those by the experiments are similar as shown in Fig.6, the concentration values quantitatively disagree between the two. However, as a result of a three-dimensional computation, it is shown that the discrepancy is caused by the way the concentration is measured in the experiment - averaging the values in the depth direction. However, as shown in Fig.9, the flow patterns obtained at planes of different depth-wise locations are quite similar among them, and also resemble the two-dimensional computational result. So, it is judged that the two-dimensional simulations are capable of capturing the basic characteristics of the flow field. In the following sections, two-dimensional simulations are used to investigate the relations between the values of indicator candidates measured in the cavity upstream and the mixing actually accomplished downstream.

### 3.3. Interface Length

Most efforts to enhance mixing have concentrated on stretching the interface between the two liquids as much as possible. It is believed that elongating the interface and providing more area for molecular diffusion to take place is the most promising way to enhance mixing. In this section, a two-dimensional numerical simulation is used to check the validity of this.

A line of tracers is introduced in to the flow field along the spanwise direction at the junction of the main channel, $x$ = 2 mm, to imitate the periodic injection of markers. The boundary between the tracers is investigated by tracking their advection and thus calculating the interface length. The mean flow velocity in the straight part of the channel is set $U$ = 5 mm/s.

The time variations of the interface length are calculated and presented in Fig.11. In the straight channel, the interface length increases linearly with time. However, in the channel

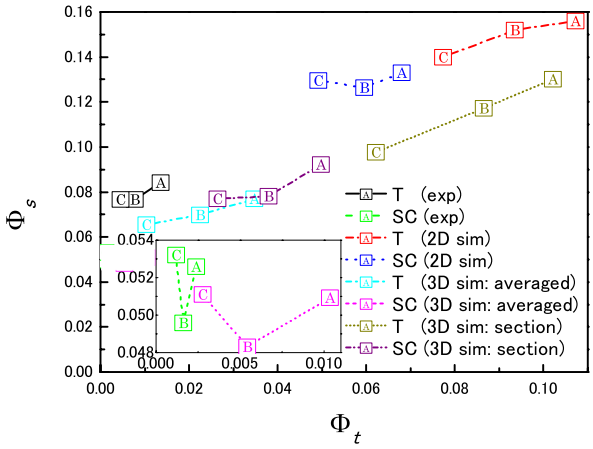


Fig. 10 Distribution of $\Phi_s$ and $\Phi_t$ at $x$ = (A)20, (B)45 and (C)75 mm.

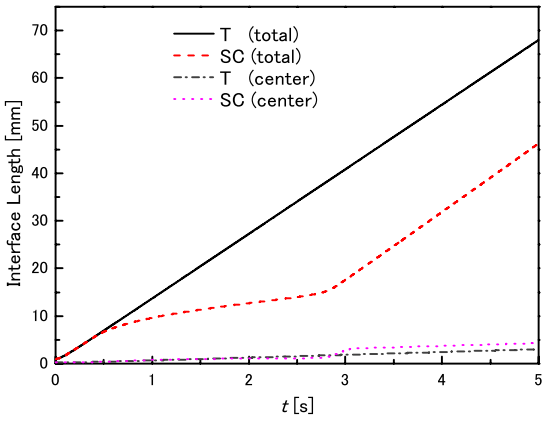


Fig. 11 Relation between the interface length and time.

with a cavity, its gradient changes suddenly at $t$ = 0.5 s, corresponding to the time when the tracers pass the inlet of the cavity, and at $t$ = 2.8 s, corresponding to the time when the tracers pass the outlet of the cavity. While the tracers are inside the cavity, the interface extends slowly. It is only after the front of the tracers passes the outlet of the cavity that the interface length increases as rapidly as the straight channel. Thus, when judged based on the interface length stretching, the straight channel without a cavity gives a better result.

Next, the behavior of tracers placed only near the center of the channel, $y = -0.1 \sim 0.1$ mm, is examined. Tracers are introduced from the same position $x$ = 2 mm. In the channel with a cavity, the tracers spread only slightly in the spanwise direction inside a cavity before they flow out. As a result, the interface length becomes only slightly larger than that in the straight channel. Their growth rates are negligible compared to the total length. This result implies that most of the extensions of the interface take place near the wall, where the velocity gradient is large.

Taking into account the fact that a channel with a cavity mixes two fluids more effectively, these results indicate that the increase in the interface length is not sufficient as an indicator to predict the mixing level downstream. In other words, focusing merely on interface extension is misleading and dangerous.

### 3.4. Interface Stretching and Concentration Gradient

Even where the stretching rate of the interface is high, significant molecular diffusion

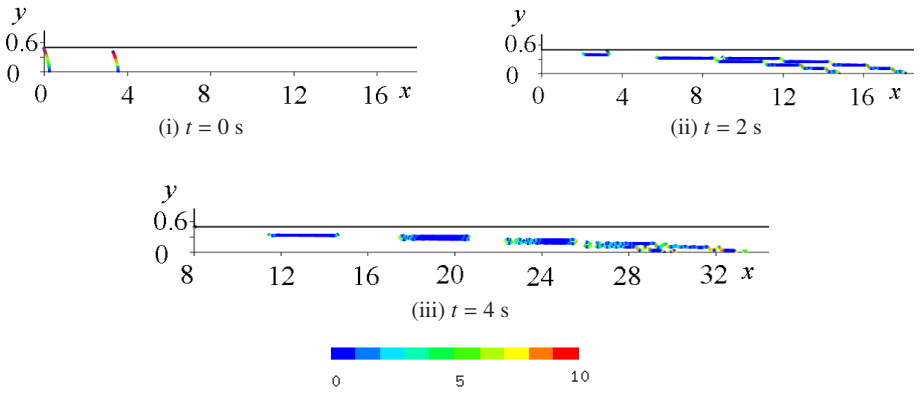


Fig. 12 Flow pattern and concentration gradient crossing interface at $t$ = 0, 2 and 4 s. (Type T)

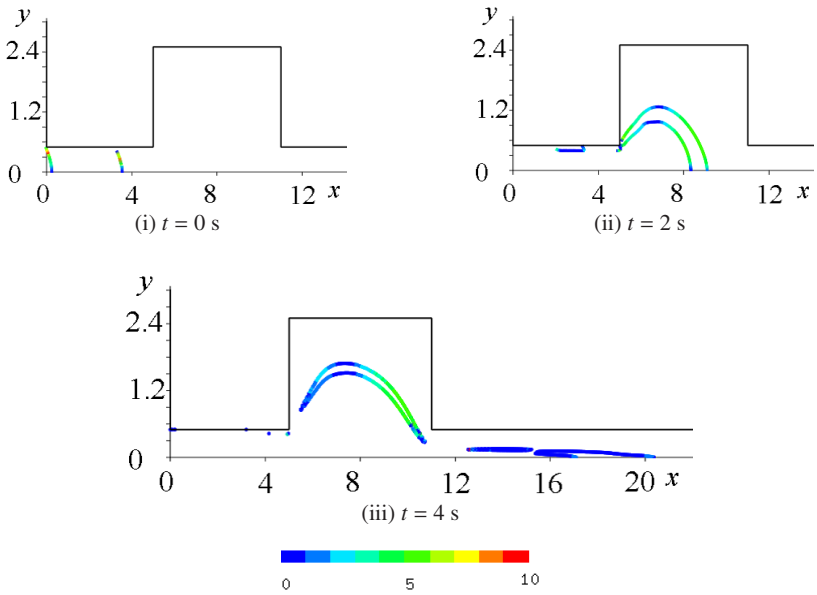


Fig. 13 Flow pattern and concentration gradient crossing interface at $t$ = 0, 2 and 4 s. (Type SC)

mixing cannot be expected if the two liquids at the location are already well mixed. In other words, stretching the interface has less meaning if the gradient of the concentration is low at the location. This situation can be observed near the side walls of the straight part of the mixing channel. A two-dimensional numerical simulation is performed for checking. The mean flow velocity is $U$ = 5 mm/s at the straight channel part. A column of water between $x = 0 \sim 3$ mm is colored, and its interface with the clear water is tracked. The interface is defined as a line with concentration of $\theta = 0.5$.

Figures 12 and 13 depict the how the patterns of colored water change. Only the upper half of the domain is displayed. In a straight channel, the concentration gradient at the interface quickly decreases while the interface is stretched with time. In contrast, in a channel with a cavity, the concentration gradient at the interface remains high while the interface is gradually stretched inside the cavity. Therefore, it can be expected that mixing between two liquids due to molecular diffusion is active there. This result explains why the cavity is effective for mixing.

## 4. Conclusions

The important factors for highly efficient mixing in an alternate inflow combined with a cavity have been studied experimentally and numerically. The main results are summarized as follows.

- The fractal dimension and the interface length provide a guideline to design a more efficient mixing channel.
- The mixing levels obtained in the experiment and those of the averaged pattern in the three-dimensional numerical simulation agree well, even quantitatively. This result explained the quantitative discrepancy between the two-dimensional computation and the experiment.
- Merely increasing the interface length is not sufficient for successful mixing. In order to achieve better mixing, the interface where the concentration gradient is high should be stretched.

## References

( 1 ) M. A. Burns, B. N. Johnson, S. N. Brahmasandra, K. Handique, J. R. Webster, M. Krishnan, T. S. Sammarco, P. M. Man, D. Jones, D. Hedsinger, C. H. Mastrangelo and D. T. Burke, An Integrated Nanoliter DNA Analysis Device, *Science*, Vol.282, (1998), pp.484-487.

( 2 ) A. Manz, N. Graber and H.M. Widmer, Miniaturized total chemical analysis systems: A novel concept for chemical sensing, *Sensors and Actuators, B*, Vol.1, (1990), pp.244-248.

( 3 ) Ottino J M, *The kinematics of mixing: stretching, chaos, and transport*, (1989), Cambridge University Press.

( 4 ) L. H. Lu, K. S. Ryu and C. Liu, A Magnetic Microstirrer and Array for Microfluidic Mixing, *J. of Microelectromechanical Systems*, Vol.11, (2002), pp.462-469.

( 5 ) R. H. Liu, J. Yang, M. Z. Pindera, M. A. Athavale and P. Grodzinski, Bubble-induced acoustic micromixing, *Lab Chip*, Vol.2, (2002), pp.151-157.

( 6 ) Z. Yang, S. Matsumoto, H. Goto, M. Matsumoto and R. Maeda, Ultrasonic micromixer for microfluidic systems, *Sensors and Actuators*, Vol.93, (2001), pp.266-272.

( 7 ) V. Mengeaud, J. Josserand and H. H. Girault, Mixing Processing in a Zigzag Microchannel, Finite Element Simurations and Optical Study, *Anal. Chem.*, Vol.74, (2002), pp.4279-4286.

( 8 ) V. Hessel, S. Hardt, H. Lowe, and F. Schönfeld, Laminar Mixing in Different Interdigital Micromixers: I. Experimental Characterization, *AIChE Journal*, Vol.49, (2003), pp.566-577.

( 9 ) A. D. Stroock, S. K. W. Dertinger, A. Ajdari, I. Mezić, H. A. Stone and G. M. Whitesides, Chaotic Mixer for Microchannels, *Science*, Vol.295, (2002), pp.647-651.

(10) S. H. Wong, M. C. L. Ward, C. W. Wharton, Micro T-mixer as a rapid mixing micromixer, *Sensors and Actuators*, Vol.100, (2004), pp.359-379.

(11) T. Kaneko, S. Izawa, A. K. Xiong, Y. Fukunishi: Mixing Enhancement of Two Liquids by Active Control in a Millimeter-scale Channel Flow, *10th Asian Congress of Fluid Mechanics, Sri Lanka*, (2004), A19 CD-ROM.

(12) K. Kokunai, T. Kaneko, S. Izawa, A. K. Xiong and Y. Fukunishi, Active control of mixing enhancement of two liquids in a millimeter-scale channel, *11th Asian Congress of Fluid Mechanics, Malaysia*, (2006), pp.480-485 CD-ROM.

(13) S. Izawa, T. Kaneko, K. Kokunai, A. K. Xiong and Y. Fukunishi, Active mixing control in a small-scale channel, *EUROMECH Fluid Mechanics Conference 6 Sweden*, (2006), pp.342 CD-ROM.

(14) T. Yabe, T. Ishizawa, P. Y. Wang, T. Aoki, Y. Kadota and F. Ikeda, A universal solver for hyperbolic equations by cubic-polynominal interpolation II. Two- and three-dimensional solvers, Compute., *Phys. Commun.*, Vol.66, (1991), pp.233-242.